

Dynamical visualization of attractively interacting single vortices in type-II/1 superconducting Nb by magneto-optical imaging

S. Ooi¹, M. Tachiki¹, T. Mochiku¹, H. Ito², T. Kubo^{2,3}, A. Kikuchi⁴, S. Arisawa⁴, and K. Umemori^{2,3}

¹International Center for Materials Nanoarchitectonics, National Institute for Materials Science, Sengen 1-2-1, Tsukuba 305-0047, Japan

²High Energy Accelerator Research Organization, 1-1 Oho, Tsukuba 305-0801, Japan

³SOKENDAI (The Graduate University for Advanced Studies), Hayama 240-0193, Japan

⁴Research Center for Energy and Environmental Materials (GREEN), National Institute for Materials Science, Sengen 1-2-1, Tsukuba 305-0047, Japan

(Received 3 April 2024; revised 5 November 2024; accepted 21 February 2025; published 19 March 2025)

In type-II/1 superconductors, the intervortex interaction has a potential minimum, resulting in an attractive force at certain distances. To better understand this unique vortex system, *in situ* observations in high-purity Nb have been performed using magneto-optical imaging with single-vortex resolution. We have dynamically visualized the behavior of the vortices during cooling, including clustering of attractively interacting single vortices, the hopping motion of vortices, the formation of an Abrikosov triangular lattice, and various degrees of disordered states with or without clusters. From the direct observations of clustering vortices, a conversion temperature for the boundary between type-II/2 and type-II/1 states is evaluated. The diverse vortex configurations arise from the interplay of the vortex-vortex interaction, the screening current, and the pinning potential landscape.

DOI: 10.1103/PhysRevB.111.094519

I. INTRODUCTION

The Ginzburg-Landau (GL) theory, basically valid near the critical temperature T_c , classifies superconductors into type I and type II. Beyond this classification, theories applicable well below T_c [1–6] further distinguish type-II superconductors into type II/1 and type II/2. Type-II/1 superconductors, with a GL parameter $\kappa < 1.1$, exhibit attractive interactions of vortices at intermediate distances, in contrast to the repulsive forces seen in type-II/2 (normal type-II) superconductors. The attraction is linked to a potential minimum of the vortex-vortex interaction at a length scale of several times of the magnetic penetration depth λ [4,7]. Initial research in the 1970s on materials such as Nb, V, TaN, and PbTi revealed these phenomena [8–12]. The origin of the attractive interaction is qualitatively understood by the condensation energy mechanism, i.e., the order parameter overlap [13]. Recently, advanced experimental studies on this issue have rekindled interest in the type-II/1 superconductors [14–17]. While there are various superconductors that have been expected to manifest attractively interacting vortices, due to different mechanisms, i.e., magnetic superconductors [18], multiband superconductors [19–21], and topological superconductors [22], type-II/1 superconductors can provide a tractable platform to study such a vortex system with less influence of pinning since the pinning effect would often mask the behavior originating from the vortex-vortex interaction.

The boundary between type II/1 and type II/2 has been evaluated numerically by solving the Eilenberger equations without an approximation [4] [for the two-dimensional (2D) case, see Ref. [23]]. The experimentally determined boundaries of the type II/1 in the κ - T diagram have been quantitatively compared with several theories in Ref. [24].

Here, we show the schematic κ - T diagram in Fig. 1(a) [11,25], and Fig. 1(b) is, as an example, the numerically calculated vortex-vortex interaction energy expected in the type-II/1 superconductivity, where the London penetration depth λ_L and κ are set to 100 nm and 0.77, respectively. The details are described in the Appendix. The first potential minimum appears at $\sim 6\lambda_L$. Interestingly, the interaction potential oscillates with reducing the amplitude [26]. The repulsive force caused by the nonmonotonic potential may prevent the vortices from coalescing into a single domain [27]. A molecular dynamics simulation using this interaction potential is demonstrated in the Supplemental Material [28] (see also Refs. [29–31] therein).

High-purity Nb of a representative type-II/1 superconductor undergoes a transition from type-II/2 to type-II/1 behavior at the conversion temperature T^* during cooling. The superconducting properties of high-purity Nb samples have been studied by magnetization measurements [8,9,32]. Without any demagnetization effect (demagnetization factor $D = 0$), a magnetization jump in H_{c1} appears in the M - H curves, indicating a first-order transition due to the attractive interaction [the orange line in Fig. 1(c)]. For $D \neq 0$ [Fig. 1(d)], instead of the first-order transition, the intermediate mixed state (IMS) appears between the Meissner and mixed states below T^* . While real-space observations of the IMS have been realized by the Bitter decoration technique [12,33], the dynamical behavior of the vortices, e.g., the emergence process of the IMS, has not been revealed due to the lack of real-time observations.

From an application perspective, the behavior of vortices in pure Nb is closely related to the performance of the superconducting radio-frequency (SRF) cavity, since remanent vortices that cannot be expelled from the cavity during cooling degrade the Q factor [34–36]. In this context, understanding

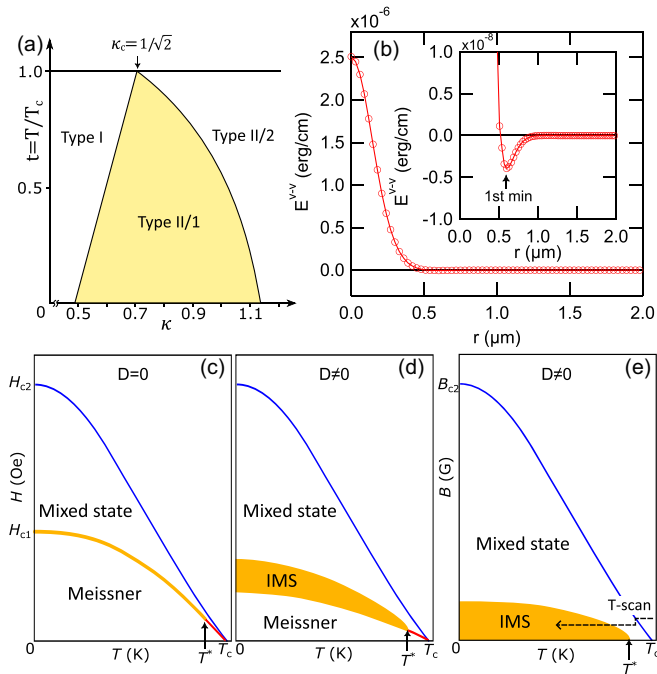


FIG. 1. (a) Schematic t - κ diagram in the vicinity of $\kappa = 1/\sqrt{2}$ based on previous papers [11,25]. Type-II/1 superconductivity exists between the type I and type II/2 (type II). (b) Calculated vortex-vortex interaction energy as a function of intervortex distance. The inset is an enlarged plot of the zero-energy region. A potential minimum, indicated by the arrow, exists at an intermediate distance. (c), (d) Schematic H - T phase diagrams of type-II/1 superconductors with demagnetization factors $D = 0$ and $D \neq 0$ for the type-II side $\kappa > 1/\sqrt{2}$. T^* is the conversion temperature which separates type-II/2 and type-II/1 behavior. (e) B - T phase diagrams for the type-II side of type-II/1 superconductors.

the mechanism of flux expulsion, where vortex clusters may be relevant, is of significant importance to improve the Q factor.

To study the dynamic behavior of vortices, magneto-optical imaging (MOI) is a powerful technique that allows real-time real-space observation of magnetic field distributions in superconductors [37]. Individual vortices have already been resolved by MOI in several groups [38–40] and even manipulated with the help of a laser beam [40]. Recently, we have visualized the formation of IMS during field cooling in cavity grade Nb using the MOI [16]. However, in that study, the behavior of vortices in lower fields could not be investigated because the resolution of the MOI at that time was not sufficient to resolve individual vortices.

In this paper, we present the dynamical visualization of attractively interacting single vortices in high-purity cavity-grade Nb using a MOI with single-vortex resolution. In our Nb samples, the conversion temperature T^* was found to be around 8.5 K. In addition, various patterns of vortex configurations emerged depending on temperature and field due to the interplay of multiple factors, i.e., the vortex-vortex interaction, the Lorentz force from a screening current, and the disordered pinning potential landscape.

II. EXPERIMENTS

Single-domain Nb samples with a square-cuboid shape of $7 \times 7 \times 3 \text{ mm}^3$ were cut from high-purity large-grain plates (Tokyo Denki Company) originally prepared for SRF cavities. The samples were annealed at 900 °C for 3 h in a vacuum of $\sim 10^{-4}$ Pa to dehydrogenate, after one side of the square surfaces was mirror polished by chemical-mechanical polishing. The residual resistance ratio (RRR) of the plates is 496 according to the data sheet provided by the company. We expected the value of κ of our Nb samples to be in the range of 0.73–0.81 [16].

The MO observations were performed using a conventional polarizing microscope setup. A schematic drawing of our low-temperature MO imaging setup is shown in Fig. 1 of Ref. [16]. In the present study, a scientific complementary metal-oxide-semiconductor (scCMOS) camera (pco.panda 4.2, Excelitas PCO GmbH) was used for image acquisition, and a high-power green light-emitting diode (LED) chip was used as a light source to enhance illumination. External magnetic fields H_z and H_x were applied perpendicular and parallel to the prepared surface, respectively, where H_x was used to roughly compensate for the in-plane ambient field. Regarding the sign of H_z (or B_z), the direction from the bottom to the top of the paper is defined as positive. The angle of rotation of the analyzer was slightly shifted from the crossed-Nicols configuration by 1° – 1.5° for better contrast [38]. Due to this angular offset, negative/positive B_z appear darker/brighter in the MO image. Therefore, a positive vortex and negative antivortex can be distinguished.

For the present study, we developed our own MO imaging sensors, which are garnet films of $(\text{Lu}, \text{Bi})_3(\text{Fe}, \text{Ga})_5\text{O}_{12}$. The films were fabricated on a gadolinium gallium garnet (GGG) substrate by an eclipse pulsed laser deposition (PLD) method [41,42], in which a shadow mask was placed between the target pellet and the substrate to prevent the deposition of large particles such as droplets. The MO film used in this study shows a zigzag pattern of magnetic domain walls at low temperatures, indicating the presence of in-plane magnetization domains. The film thickness is ~ 500 nm estimated from the total deposition time.

All images were taken during field cooling (T scan). Since the MOI signal reflects the local flux density B_l , it is convenient to use a B - T plot to follow the T scan [Fig. 1(e)], where a typical change in B_l is indicated by the arrow [16]. A sudden decrease of B_l occurs at T_c due to the flux expulsion. To enhance the contrast of the images, the background image, which is an average of several dozen images taken above T_c , was subtracted from all successive images after image registration to remove non-negligible drift or vibration, and a Gaussian filter was applied to reduce noise.

III. RESULTS AND DISCUSSION

Figure 2 shows MO images taken during the T scan in -9.3 Oe. Note that the temperature shown in the images has an error about ± 0.05 K due to temperature instability in our experimental setup. Just below T_c around 9.2 K many uniform dark spots appear (see Video 1 in the Supplemental Material [28]), which is the creation of (anti)vortices. By

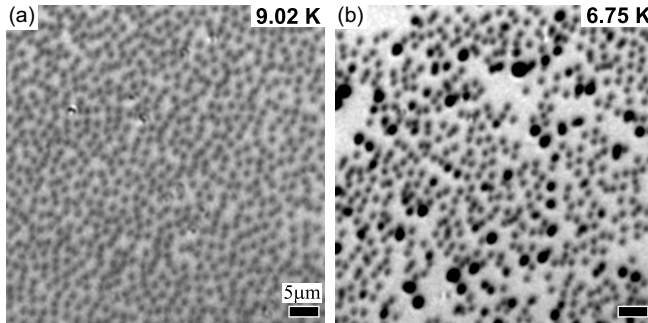


FIG. 2. (a) MO image of single vortices at 9.0 K below T_c during the T scan in -9.3 Oe. Since the MO film senses the magnetic field a few submicrons above the sample surface and there are other factors such as image processing, contrast adjustment, etc., the size of the vortices appears larger. (b) MO image of clustering vortices below the conversion temperature T^* . The video is available in the Supplemental Material [28].

counting the number of vortices in Fig. 2(a), B is estimated to be -5.1 G. As the temperature decreases, slight drifts of the vortices from left to right can be seen down to 8.7 K, indicating the influence of the Lorentz force exerted by the screening current. In addition, a hopping motion of the vortices can be seen, suggesting that pinning by some amount of quenched disorder exists at least at the surface, although the sample is sufficiently clean for IMS to appear at low temperatures.

With a further decrease temperature, the vortices begin to aggregate at ~ 8.5 K, forming vortex clusters. The clusters gradually grow by absorbing other vortices around them. As shown in Fig. 2(b), not all vortices are involved in cluster formation. This is probably caused by the competition of the attractive force between vortices and the pinning force. Since the MO image shows the vortex pattern on the surface, there is a possibility that some of the isolated single vortices are pinned at the surface and may cluster in the body of the sample if the effective pinning centers exist only near the surface.

Recently, the expectation that ideal pure Nb is an intrinsic type-I superconductor has been proposed, in which the similarity of magnetic field patterns of the IMS in Nb and the intermediate state in Pb was thought to be a supporting evidence [43]. Since the spatial resolution of our MOI is insufficient to reveal the internal structure of the cluster, we cannot exclude the possibility that the “vortex cluster” here is a “giant vortex.” However, recent small-angle neutron scattering studies using Nb samples of different purities with RRRs of ~ 100 (“Nb-lp”), > 300 (“Nb-mp”), and $> 10\,000$ (“Nb-hp”) have observed Bragg spots of a hexagonal lattice of single vortices below the temperature of the aggregation in all cases. The purity of our Nb samples ($\text{RRR} \sim 500$) is probably between Nb-mp and Nb-hp, and the transition temperature to IMS, T_{IMS} , is also between Nb-mp and Nb-hp in fixed magnetic fields [15,16], suggesting that the quality of the current samples does not reach ideal pure Nb. Therefore, the observed aggregate structure of vortices is expected to be a “vortex cluster.” Further direct observation studies for much higher-purity Nb with a better spatial resolution than several hundreds nm are required to explore the type-I superconducting Nb.

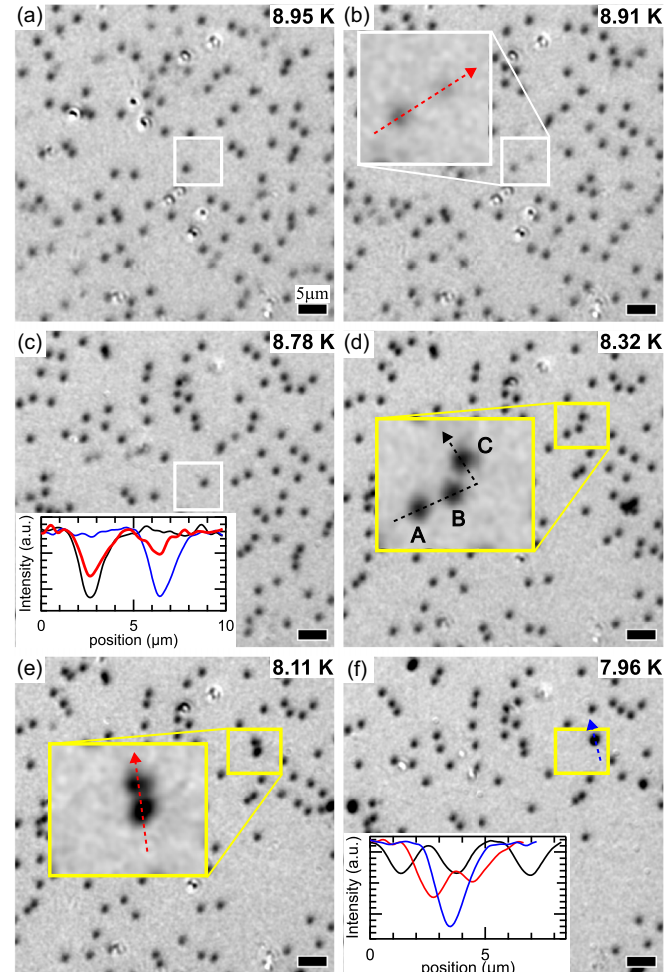


FIG. 3. MO images taken in -2.3 Oe during the T scan. (a)–(c) Sequential images of a hopping vortex (in the white box). Black, red, and blue lines in the inset of (c) show line profiles of the vortex in (a)–(c), respectively, along the red arrow in (b). (d)–(f) Clustering of three vortices (in the yellow box). The line profiles along the arrows drawn in the figures are plotted in the inset of (f). The video is available in the Supplemental Material [28].

Snapshots during the T scan in a lower field (-2.3 Oe) are shown in Fig. 3. There is an overall flow towards 2 o’clock just below T_c , where the hopping motion of the vortices can be seen again in Figs. 3(a)–3(c). The two dark spots in the white box of Fig. 3(b) are a trace of a hopping single vortex, indicating an instantaneous jump during the exposure time of 0.5 s, whose profiles are shown in the inset of Fig. 3(c). The ratio of the intensities of two negative peaks reflects that of the dwell times at the two positions.

In Fig. 3, most of the vortices remain isolated single vortices even well below 8.5 K, probably because the vortices are too far apart to attract each other against the pinning force. However, in the yellow box in Figs. 3(d)–3(f), we can find three vortices, labeled A, B, and C, forming clusters: The vortex A collides with the second vortex B, and then the cluster consisting of A and B becomes attached with C. Their profiles are shown in the inset of Fig. 3(f). The clusters appear to form and grow by collisions of vortices during hopping.

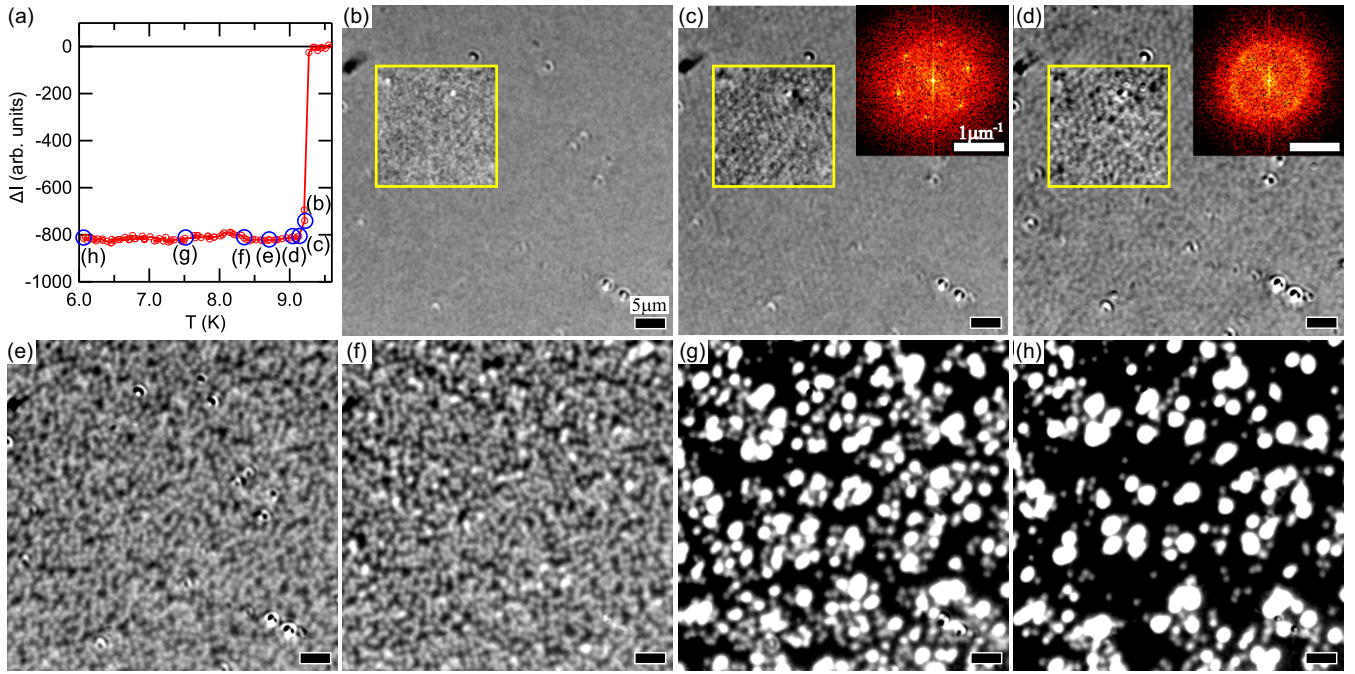


FIG. 4. Vortex arrangement during the T scan in a relatively higher field. (a) Change in averaged light intensity ΔI from the value above T_c during the T scan in 15.7 Oe. Labels (b)–(h) indicate the points corresponding to the following images. (b)–(h) Successive changes of the vortex arrangements: (b) An image just below T_c (9.2 K), (c) ordered vortex lattice (9.1 K), (d) weakly disordered state (9.1 K), (e) strongly disordered state (8.7 K), and (f)–(h) intermediate mixed state (8.4, 7.5, and 6.1 K, respectively). The insets of (c) and (d) show the results of the FFT for each image. All images are displayed with a fixed grayscale, except for the regions surrounded by yellow squares in (b)–(d), where the contrasts are increased for visibility. The video is available in the Supplemental Material [28].

Figure 4 shows the changes of the vortex arrangement during the T scan in a relatively higher field (+15.7 Oe), where single vortices are still resolved. Note that the vortices are represented by bright spots, unlike those in Figs. 2 and 3 because their fields are positive. Just after the superconducting transition, a certain amount of magnetic field is expelled from the sample, as shown in Fig. 4(a), but there is no sign of vortices in Fig. 4(b), probably because the field modulation by vortices is small, since $\lambda(T)$ should be longer, much closer to T_c . In the next image [Fig. 4(c)], despite a small decrease in temperature, we notice the appearance of an ordered vortex lattice, which is a hexagonal lattice with a lattice constant of $\sim 1.5 \mu\text{m}$, corresponding to 11 G, from the result of the fast Fourier transformation (FFT). However, this ordered lattice is broken within a small temperature decrease [Fig. 4(d)]. This change is probably due to the interplay of the weak intervortex interaction, the pinning effect, and the Lorentz force due to the screening current. Since the vortex lattice is too soft near $B_{c2}(T)$ or in very low fields [44,45] to maintain the ordering, some vortices move downward due to the Lorentz force while others appear to be fixed. With decreasing temperature the arrangement is further disordered [Fig. 4(e)]. Then, below ~ 8.5 K, the vortices suddenly start to form clusters as shown in Fig. 4(f), indicating that the attractive force between the vortices overcomes the pinning force around this temperature. As the temperature continues to decrease, the clusters gradually absorb the individual vortices around them [Fig. 4(g)]. At low temperatures [Fig. 4(h)], some vortices remain isolated from the clusters,

suggesting the existence of relatively strong pinning centers in this sample.

From the consecutive images in the T scan, we extracted some characteristic temperatures, i.e., the starting temperature of the clustering T_{cluster} , temperatures where the vortex lattice is observed T_{lattice} , and the superconducting transition temperature T_{c2} , which are illustrated in Fig. 5. T_{lattice} gradually shifts toward lower temperatures as the magnetic field increases, because the vortex lattice becomes stiffer as the intervortex distance decreases, maintaining the ordered structure at lower temperatures against the temperature-dependent pinning force. On the other hand, T_{cluster} seems to be independent of the magnetic field and concentrate around 8.5 K, indicating that the conversion temperature T^* is around this value, although they are somewhat scattered due to the ambiguity of the manual determination and the limited experimental stability of the temperature. It is possible that the influence of the pinning remaining in our Nb sample has led to an underestimation of T^* . However, it is expected that even under the influence of pinning, clustering could occasionally occur as a result of a collision between the weakly pinned mobile vortices when the attractive force starts to work. Since there is no clear case of clustering vortices above ~ 8.5 K for the different fields, we expect T^* to be around 8.5 K in this sample.

The conversion temperature is an important parameter to investigate the superconducting property of Nb including the quality of samples via the relationship between T^* and κ . In previous experiments T^* has been evaluated by examining the

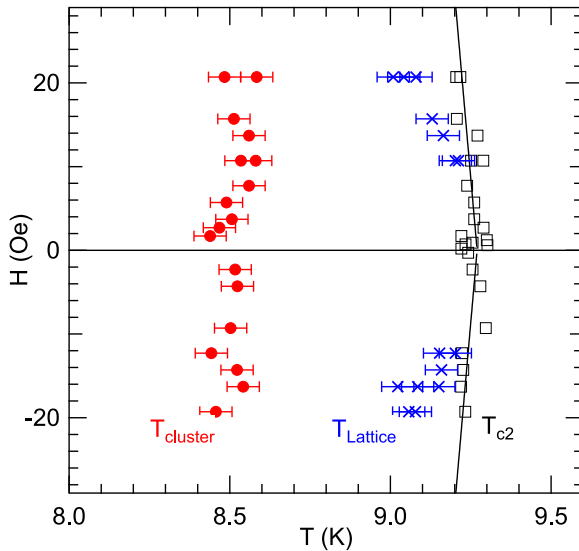


FIG. 5. Plot of several characteristic temperatures determined from the observations in T scan. Red circles, T_{cluster} , show the temperature at which vortices start to aggregate. Crossed markers, T_{lattice} , indicate the point where the vortex lattices were detected. The superconducting transition temperature $T_{\text{c}2}$ is also shown by black squares with a line of $H_{\text{c}2}(T) = 4040(1 - t^2)/(1 + t^2)$, where $t = T/T_{\text{c}}$ and T_{c} is 9.25 K [46].

magnetization jump accompanied by the first vortex penetration in the M - H curves in sample shapes of $D \sim 0$ [8] or by detecting slope changes by the differential magnetization using large- D samples [24,24]. However, these macroscopic methods may give an error in lower fields and higher temperatures due to the reduced number of vortices involved. Direct observation by MOI can be an alternative means to determine T^* , especially for low fields as demonstrated in the present study, and applicable to platelike shapes.

IV. CONCLUSION

In conclusion, we have successfully conducted a dynamical observation of attractively interacting single vortices in low fields (< 20 Oe) in high-purity cavity-grade Nb using a MOI with single-vortex resolution. In our Nb sample, the conversion temperature T^* was found to be about 8.5 K. During field cooling, in addition to the hopping motion of single vortices, the diverse vortex configurations, such as a hexagonal lattice, a weakly or strongly disordered state, and a mixture of isolated vortices and clusters, were observed depending on temperature and field, which can be explained by the combined influence of multiple factors, i.e., the vortex-vortex interaction, the Lorentz force from the screening current, and the disordered landscape of the pinning potential. As a future prospect, further improvement of the spatial, temporal, and magnetic resolutions in the MOI will make it possible to dynamically study the internal structure of vortex clusters, vortex lattice structures in higher fields, or the birth of vortices just at T_{c} .

ACKNOWLEDGMENTS

The authors would like to thank T. Konomi, S. Yoshizawa, E. Kako, H. Sakai, K. Tsuchiya, and K. Hirata for their close collaboration and advice. This study was supported by JSPS KAKENHI Grant No. 23K03329 and partially by JSPS KAKENHI Grant No. 21K04145.

DATA AVAILABILITY

The data that support the findings of this article are openly available [47].

APPENDIX: ATTRACTIVE VORTEX-VORTEX INTERACTION

The attractive vortex-vortex interaction is not described by the conventional GL theory. Several approaches have been studied to go beyond the GL theory to investigate the vortices in a type-II/1 superconductor [1,3–5]. On the other hand, the boson method is the quantum field theory suitable to treat the topological defects in an ordered state (e.g., vortices in superconductors) [48,49], and the theory of superconductivity has been formulated based on this formalism [2,50]. Here, we use the vortex-vortex interaction formulas by the boson method of superconductivity to study the attractive vortex behavior and vortex cluster formation [2,26,51].

The vortex-vortex interaction potential energy and force (per unit length) are expressed as follows, respectively [2,51],

$$E^{\text{v-v}}(r) = \frac{\phi_0^2}{8\pi^2} \int_0^\infty \frac{kc(k)J_0(kr)}{\lambda_L^2 k^2 + c(k)} dk, \quad (\text{A1})$$

$$|\mathbf{F}^{\text{v-v}}(r)| = \frac{\phi_0^2}{8\pi^2} \int_0^\infty \frac{k^2 c(k)J_1(kr)}{\lambda_L^2 k^2 + c(k)} dk, \quad (\text{A2})$$

where r is the distance between the axes of the two vortices, ϕ_0 is the unit flux quantum, λ_L is the London penetration depth, and J_0, J_1 are the zeroth- and first-order Bessel functions, respectively. $c(k)$ is the so-called boson characteristic function. $c(k)$ at $T = 0$ K has been calculated numerically as follows [26]: $c(k) = \exp\{-\nu[k\xi_0]^\eta\}$ where ξ_0 is the coherence length, $\nu = 0.559 - 0.4257VN(0)$, $\eta = 2.207 - 0.7857VN(0)$. V is the coupling constant of the electron-electron interaction. $N(0)$ is the density of state at the Fermi level. We adopted 0.32 for $VN(0)$ to follow Ref. [26].

The numerically calculated vortex-vortex interaction energy as a function of the distance between two vortices with the values λ_L of 100 nm and κ of 0.77 is shown in Fig. 6. $E^{\text{v-v}}(r)$ is an oscillatory damped function [26], which can be seen up to the second minimum in Fig. 6(c).

Boson methods start from the Bardeen-Cooper-Schrieffer (BCS) Hamiltonian, but instead of formulating using the Green's function in the manner of the Gor'kov equations,

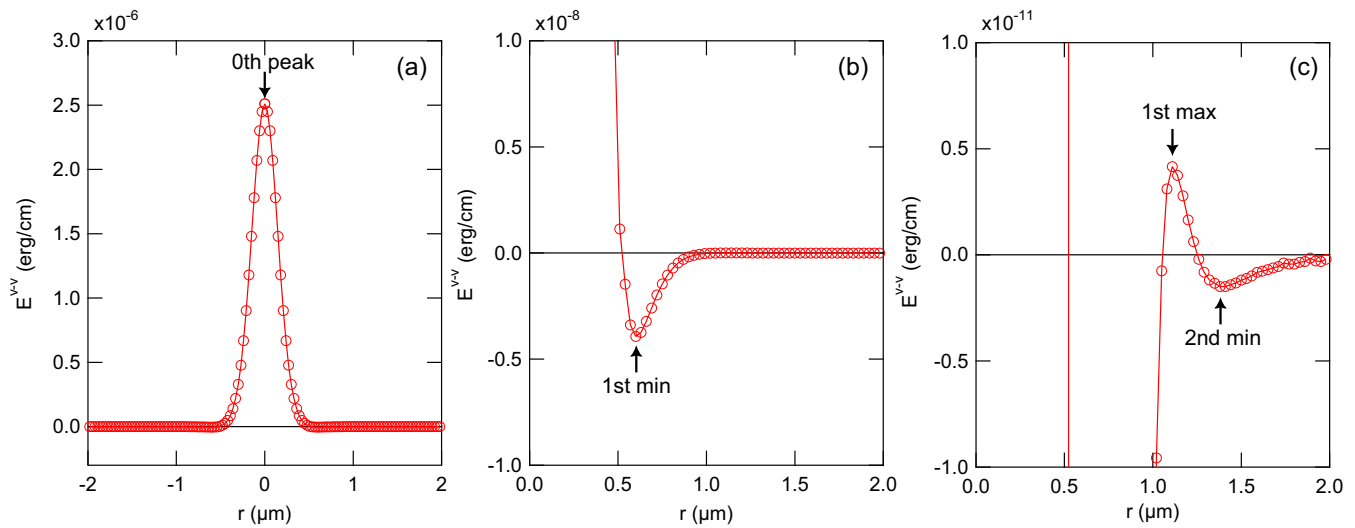


FIG. 6. Calculated potential energy of the vortex-vortex-interaction: (a) Central peak (“0th peak”). (b) Around the first minimum. (c) Around the first maximum and the second minimum.

they advance through the operator formalism to be derived. Although they should be consistent with other theoretical

frameworks through the BCS Hamiltonian, this remains a topic for future research.

- [1] G. Eilenberger and H. Büttner, The structure of single vortices in type II superconductors, *Z. Phys.* **224**, 335 (1969).
- [2] L. Leplae, H. Umezawa, and F. Mancini, Derivation and application of the boson method in superconductivity, *Phys. Rep.* **10**, 151 (1974).
- [3] E. H. Brandt, Microscopic theory of clean type-II superconductors in the entire field-temperature plane, *Phys. Status Solidi B* **77**, 105 (1976).
- [4] U. Klein, Microscopic calculations on the vortex state of type II superconductors, *J. Low Temp. Phys.* **69**, 1 (1987).
- [5] T. Koyama and M. Machida, Nonlocal Ginzburg-Landau theory for superconductors, *Phys. C: Superconductivity* **484**, 100 (2013).
- [6] V. D. Neverov, A. E. Lukyanov, A. V. Krasavin, A. A. Shanenko, M. D. Croitoru, and A. Vagov, Microscopic description of intermediate mixed state in superconductors between the first and second types, *Phys. Rev. B* **110**, 054502 (2024).
- [7] E. H. Brandt, The flux-line lattice in superconductors, *Rep. Prog. Phys.* **58**, 1465 (1995).
- [8] D. K. Finnemore, J. R. Clem, and T. F. Stromberg, Attractive interaction between vortices in Nb, *Phys. Rev. B* **6**, 1056 (1972).
- [9] J. J. Wollan, K. W. Haas, J. R. Clem, and D. K. Finnemore, Phase transition at $H_{\text{c}1}$ for superconducting Nb and V, *Phys. Rev. B* **10**, 1874 (1974).
- [10] J. Schelten, H. Ullmaier, and W. Schmatz, Neutron diffraction by vortex lattices in superconducting Nb and $\text{Nb}_{0.73}\text{Ta}_{0.27}$, *Phys. Status Solidi B* **48**, 619 (1971).
- [11] J. Auer and H. Ullmaier, Magnetic behavior of type-II superconductors with small Ginzburg-Landau parameters, *Phys. Rev. B* **7**, 136 (1973).
- [12] U. Krägeloh, Flux line lattices in the intermediate state of superconductors with Ginzburg-Landau parameters near 12, *Phys. Lett. A* **28**, 657 (1969).
- [13] U. Klein, L. Kramer, W. Pesch, D. Rainer, and J. Rammer, Microscopic calculations of vortex structure and magnetization curves for type II superconductors, *Acta Phys. Hung.* **62**, 27 (1987).
- [14] T. Reimann, M. Schulz, D. F. R. Mildner, M. Bleuel, A. Brûlet, R. P. Harti, G. Benka, A. Bauer, P. Böni, and S. Mühlbauer, Domain formation in the type-II/1 superconductor niobium: Interplay of pinning, geometry, and attractive vortex-vortex interaction, *Phys. Rev. B* **96**, 144506 (2017).
- [15] A. Backs, M. Schulz, V. Pipich, M. Kleinhans, P. Böni, and S. Mühlbauer, Universal behavior of the intermediate mixed state domain formation in superconducting niobium, *Phys. Rev. B* **100**, 064503 (2019).
- [16] S. Ooi, M. Tachiki, T. Konomi, T. Kubo, A. Kikuchi, S. Arisawa, H. Ito, and K. Umemori, Observation of intermediate mixed state in high-purity cavity-grade Nb by magneto-optical imaging, *Phys. Rev. B* **104**, 064504 (2021).
- [17] X. S. Brems, S. Mühlbauer, and R. Cubitt, Pushing the limits of accessible length scales via a modified Porod analysis in small-angle neutron scattering on ordered systems, *J. Appl. Cryst.* **57**, 1358 (2024).
- [18] M. Tachiki, H. Matsumoto, and H. Umezawa, Mixed state in magnetic superconductors, *Phys. Rev. B* **20**, 1915 (1979).
- [19] V. Moshchalkov, M. Menghini, T. Nishio, Q. H. Chen, A. V. Silhanek, V. H. Dao, L. F. Chibotaru, N. D. Zhigadlo, and J. Karpinski, Type-1.5 superconductivity, *Phys. Rev. Lett.* **102**, 117001 (2009).
- [20] S.-Z. Lin and X. Hu, Vortex states and the phase diagram of a multiple-component Ginzburg-Landau theory with competing repulsive and attractive vortex interactions, *Phys. Rev. B* **84**, 214505 (2011).
- [21] E. Babaev, J. Carlström, J. Garaud, M. Silaev, and J. Speight, Type-1.5 superconductivity in multiband systems: Magnetic

- response, broken symmetries and microscopic theory—A brief overview, *Phys. C: Superconductivity* **479**, 2 (2012).
- [22] M. Tachiki and H. Koizumi, Vortex state of topological superconductor $\text{Cu}_x\text{Bi}_2\text{Se}_3$, *Phys. Rev. B* **91**, 104505 (2015).
- [23] P. Miranović and K. Machida, Thermodynamics and magnetic field profiles in low- κ type-II superconductors, *Phys. Rev. B* **67**, 092506 (2003).
- [24] H. W. Weber, M. Botlo, F. M. Sauerzopf, H. Wiesinger, and U. Klein, Phase transitions between type-I, type-II/1 and type-II/2 superconductivity, *Jpn. J. Appl. Phys.* **26**, 917 (1987).
- [25] N. Kimura, N. Kabeya, K. Saitoh, K. Satoh, H. Ogi, K. Ohsaki, and H. Aoki, Type II/1 superconductivity with extremely high H_{c3} in noncentrosymmetric LaRhSi_3 , *J. Phys. Soc. Jpn.* **85**, 024715 (2016).
- [26] F. Mancini, R. Teshima, and H. Umezawa, Order of phase transition between the Meissner state and the mixed state, *Solid State Commun.* **24**, 561 (1977).
- [27] X. B. Xu, H. Fangohr, Z. H. Wang, M. Gu, S. L. Liu, D. Q. Shi, and S. X. Dou, Vortex dynamics for low- κ type-II superconductors, *Phys. Rev. B* **84**, 014515 (2011).
- [28] See Supplemental Material at <http://link.aps.org/supplemental/10.1103/PhysRevB.111.094519> for molecular dynamics simulations using the interaction of Eq. (A2), and descriptions of the videos provided, which includes Refs. [29–31].
- [29] COMSOL Multiphysics®, COMSOL AB, Stockholm, Sweden, www.comsol.com.
- [30] J. Schindelin, I. Arganda-Carreras, E. Frise, V. Kaynig, M. Longair, T. Pietzsch, S. Preibisch, C. Rueden, S. Saalfeld, B. Schmid, J.-Y. Tinevez, D. J. White, V. Hartenstein, K. Eliceiri, P. Tomancak, and A. Cardona, Fiji: An open-source platform for biological-image analysis, *Nat. Methods* **9**, 676 (2012).
- [31] MATLAB version 9.11.0 (R2021b), The MathWorks Inc., Natick, MA, 2021, <https://www.mathworks.com>.
- [32] H. W. Weber, E. Seidl, M. Botlo, C. Laa, E. Mayerhofer, F. M. Sauerzopf, R. M. Schalk, H. P. Wiesinger, and J. Rammer, Magnetization of low- k superconductors. I. The phase-transition at H_{c1} , *Phys. C: Superconductivity* **161**, 272 (1989).
- [33] U. Essmann, Observation of the mixed state, *Physica* **55**, 83 (1971).
- [34] A. Gurevich and G. Ciovati, Effect of vortex hotspots on the radio-frequency surface resistance of superconductors, *Phys. Rev. B* **87**, 054502 (2013).
- [35] S. Huang, T. Kubo, and R. L. Geng, Dependence of trapped-flux-induced surface resistance of a large-grain Nb superconducting radio-frequency cavity on spatial temperature gradient during cooldown through T_c , *Phys. Rev. Accel. Beams* **19**, 082001 (2016).
- [36] S. Posen, M. Checchin, A. C. Crawford, A. Grassellino, M. Martinello, O. S. Melnychuk, A. Romanenko, D. A. Sergatskov, and Y. Trenikhina, Efficient expulsion of magnetic flux in superconducting radiofrequency cavities for high Q_0 applications, *J. Appl. Phys.* **119**, 213903 (2016).
- [37] A. A. Polyanskii, P. J. Lee, A. Gurevich, Z.-H. Sung, and D. C. Larbalestier, Magneto-optical study high-purity niobium for superconducting RF application, *AIP Conf. Proc.* **1352**, 186–202 (2011).
- [38] P. E. Goa, H. Hauglin, Å. A. F. Olsen, M. Baziljevich, and T. H. Johansen, Magneto-optical imaging setup for single vortex observation, *Rev. Sci. Instrum.* **74**, 141 (2003).
- [39] Y. Tsuchiya, Y. Nakajima, and T. Tamegai, Development of surface magneto-optical imaging method, *Phys. C: Superconductivity* **470**, 1123 (2010).
- [40] I. S. Veshchunov, W. Magrini, S. V. Mironov, A. G. Godin, J.-B. Trebbia, A. I. Buzdin, P. Tamarat, and B. Lounis, Optical manipulation of single flux quanta, *Nat. Commun.* **7**, 12801 (2016).
- [41] K. Kinoshita, H. Ishibashi, and T. Kobayashi, Improved surface smoothness of $\text{YBa}_2\text{Cu}_3\text{O}_y$ films and related multilayers by ArF excimer laser deposition with shadow mask “eclipse method”, *Jpn. J. Appl. Phys.* **33**, L417 (1994).
- [42] M. Tachiki, M. Noda, K. Yamada, and T. Kobayashi, SrTiO_3 films epitaxially grown by eclipse pulsed laser deposition and their electrical characterization, *J. Appl. Phys.* **83**, 5351 (1998).
- [43] R. Prozorov, M. Zarea, and J. A. Sauls, Niobium in the clean limit: An intrinsic type-I superconductor, *Phys. Rev. B* **106**, L180505 (2022).
- [44] E. H. Brandt, On the shear modulus of the flux line lattice, *Phys. Status Solidi B* **77**, 551 (1976).
- [45] G. Blatter, M. V. Feigel'man, V. B. Geshkenbein, A. I. Larkin, and V. M. Vinokur, Vortices in high-temperature superconductors, *Rev. Mod. Phys.* **66**, 1125 (1994).
- [46] D. K. Finnemore, T. F. Stromberg, and C. A. Swenson, Superconducting properties of high-purity niobium, *Phys. Rev.* **149**, 231 (1966).
- [47] <https://doi.org/10.48505/nims.5348>.
- [48] H. Umezawa, H. Matsumoto, and M. Tachiki, *Thermo Field Dynamics and Condensed States* (North-Holland, Amsterdam, 1982).
- [49] H. Umezawa, *Advanced Field Theory: Micro, Macro, and Thermal Physics* (American Institute of Physics Press, New York, 1993).
- [50] H. Matsumoto and H. Umezawa, A rigorous formulation of the boson method in superconductivity, *Fortschr. Phys.* **24**, 357 (1976).
- [51] M. Fusco-Girard, U. Klein, and F. Mancini, Attractive interaction between the surface of a type-II superconductors and a single flux line, *Physica B+C* **107**, 423 (1981).